© 2016. Published by The Company of Biologists Ltd | Journal of Experimental Biology (2016) 219, 676-685 doi:10.1242/jeb.128652

RESEARCH ARTICLE

Exceptional running and turning performance in a mite

Samuel Rubin[1], Maria Ho-Yan Young[2], Jonathan C. Wright[2,*], Dwight L. Whitaker[3] and Anna N. Ahn[4]

ABSTRACT

The Southern California endemic mite *Paratarsotomus macropalpis* was filmed in the field on a concrete substrate and in the lab to analyze stride frequency, gait and running speed under different temperature conditions and during turning. At ground temperatures ranging from 45 to 60°C, mites ran at a mean relative speed of 192.4±2.1 body lengths (BL) s^{-1}, exceeding the highest previously documented value for a land animal by 12.5%. Stride frequencies were also exceptionally high (up to 135 Hz), and increased with substrate temperature. Juveniles exhibited higher relative speeds than adults and possess proportionally longer legs, which allow for greater relative stride lengths. Although mites accelerated and decelerated rapidly during straight running (7.2±1.2 and −10.1±2.1 m s^{-2}, respectively), the forces involved were comparable to those found in other animals. *Paratarsotomus macropalpis* employs an alternating tetrapod gait during steady running. Shallow turns were accomplished by a simple asymmetry in stride length. During tight turns, mites pivoted around the tarsus of the inside third leg (L3), which thus behaved like a grappling hook. Pivot turns were characterized by a 42% decrease in turning radius and a 40% increase in angular velocity compared with non-pivot turns. The joint angle amplitudes of the inner L2 and L3 were negligible during a pivot turn. While exceptional, running speeds in *P. macropalpis* approximate values predicted from inter-specific scaling relationships.

KEY WORDS: *Paratarsotomus*, Relative speed, Stride frequency, Gait, Turning

INTRODUCTION

Walking and running arachnids generally utilize variations on an alternating tetrapod gait, in which opposite legs are 180 deg out of phase in the stepping cycle and four legs (L1, L3, R2, R4, or L2, L4, R1, R3) contact the ground in stance phase at any given time (Spagna and Peattie, 2012). This gait structure, combined with the sprawled posture typical of most arachnid orders, provides both high static stability and maneuverability (Jindrich and Full, 1999; Weihmann, 2013). Although there is a growing body of work on spider locomotion and kinematics, much less is known about locomotion in mites (Subclass Acari). Mites offer interesting comparisons to other running arthropods, not only because of their small size and correspondingly high stride frequencies but also because of the ability of many species to run rapidly and execute tight turns while traveling over extremely uneven substrates.

[1]Department of Chemical and Systems Biology, Stanford University School of Medicine, Stanford, CA 94305, USA. [2]Department of Biology, Pomona College, Claremont, CA 91711, USA. [3]Department of Physics, Pomona College, Claremont, CA 91711, USA. [4]Department of Biology, Harvey Mudd College, Claremont, CA 91711, USA.

*Author for correspondence (jcw04747@pomona.edu)

Received 16 July 2015; Accepted 14 December 2015

Mites attain some of the fastest relative speeds documented in the animal kingdom (Wu et al., 2010). Very small mites (<1 mg) represent some of the smallest running arthropods and, as such, they allow us to test whether models relating running speed and stride frequency to animal mass apply at lower mass extremes. Both relative speed (v_r) and stride frequency (f) scale negatively with body mass (M_b) (Alexander, 1982; Weyand et al., 2000; Iriarte-Díaz, 2002; Biewener, 2003; Wu et al., 2010). Dynamic similarity and the length–resonance relationship predict that $f \propto l^{-0.5}$, where l is leg length, as for a pendulum (Alexander and Jayes, 1983; Biewener, 2003; Hurlbert et al., 2008). Assuming isometric scaling of l and M_b ($l \propto M_b^{0.33}$), we can derive the predicted scaling of stride frequency and body mass as $f \propto M_b^{-0.17}$. Similarly, absolute speed (u) should scale as $M_b^{0.17}$ ($M_b^{-0.17} \times M_b^{0.33}$) and v_r should scale as $M_b^{-0.17}$ ($M_b^{0.17}/M_b^{0.33}$). Early work showed that this predicted scaling for v_r holds true for East African mammals (Pennycuick, 1975), and this was subsequently corroborated for other mammals (Garland, 1983). More recently, however, Iriarte-Díaz (2002) showed that mammals can be subdivided into smaller species (<30 kg) with a lower v_r:M_b exponent of −0.09, and larger species with a considerably larger exponent (−0.46). Several factors may account for different exponent values and size-dependent changes in the exponent, including non-isometric scaling of limb length, metabolic power (Schmidt-Nielsen, 1984; Jones and Lindstedt, 1993), and the interaction of metabolic power and dynamic similarity constraints (Hurlbert et al., 2008).

The negative scaling of v_r and f with body mass appears to hold true for other terrestrial taxa (Biewener, 2003; Full, 2011). However, scaling models based on vertebrates may not provide good predictors for behavior in very small animals below 1 g in mass. Here, predicted stride frequency may be limited by one or more components of muscle physiology and force generation: excitation–contraction coupling, actin–myosin cross-bridge cycling, and calcium-clearance required for muscle relaxation. Alternatively, the force–velocity trade-off for muscles could limit running speed and stride frequency at small sizes. Faster muscles not only generate less force as a result of faster cross-bridge cycling, as depicted in a typical force–velocity curve, but also tend to incorporate fewer contractile myofibrils. In ultrafast muscle fibers, the rapid cross-bridge cycling depends on high mitochondrial density to sustain the rapid ATP turnover, and the fast calcium clearance required for rapid relaxation depends on a large relative volume of sequestering sarcoplasmic reticulum (SR) (Appelt et al., 1991; Rome, 2006). Both mitochondria and SR compete for space with myofibrils, but how their relative volumes scale with muscle speed is unknown.

Paratarsotomus macropalpis (Banks, 1916) is an erythracarid mite occurring in the coastal sage scrub of Southern California (Otto, 2000). This species is known for its exceptional thermal tolerance (Wu and Wright, 2015) and locomotory performance (Wu et al., 2010), with relative speeds of up to 133 BL s^{-1} and stride frequencies of up to 111 Hz at 45°C. Here, we build on previous work, using kinematic analysis of mites running on concrete substrates in the field to quantify running performance in

Journal of Experimental Biology

Journal of Experimental Biology (2016) 219, 676-685 doi:10.1242/jeb.128652

List of symbols and abbreviations

BL	body length
C_D	drag coefficient
f	stride frequency
F'	drag force per unit length
F_{drag}	drag force
Fr	Froude number
g	acceleration due to gravity
k	constant that depends on body shape (3π for a sphere, such as a mite)
l	leg length
M_b	body mass
Re	Reynolds number
u	absolute speed
u_l	leg speed
v_r	relative speed
V_{sphere}	volume of a sphere
η	dynamic viscosity
ρ	density
ϕ	leg diameter
ω	angular velocity

undisturbed animals, and lab filming to analyze stride frequency and gait structure during straight running, acceleration and turning. We also analyze the effects of body size on stride frequency and relative speed among other fast-running species to see whether observed allometric scaling provides good predictions for running speed in *P. macropalpis*. Recently published data for arachnids (Spagna and Peattie, 2012) allow a comparison of relative speeds across multiple arachnid species, as well as among other terrestrial arthropods and vertebrates. In accordance with inter-specific scaling, we hypothesize that juvenile mites will utilize higher stride frequencies and attain higher relative speeds than their adult counterparts.

MATERIALS AND METHODS

Adult and juvenile *P. macropalpis* mites were filmed running in the lab and outdoors on concrete substrates in Claremont, CA, USA. Concrete served as a sufficiently light background to provide contrast for the mites during filming. Lab filming used a plastic Petri dish or a larger enameled dish warmed with an incandescent lamp. Footage was captured using a high-speed CCD camera (Motion HG-100K, MotionXtra, RedLake, Tucson, AZ, USA) at 1000 frames s^{-1}. For outdoor filming, the camera was mounted vertically to a wheeled cart, allowing for easy movement while keeping it at a uniform distance from the ground surface. Calibration frames were recorded using a millimeter scale placed on the same substrate, and were used to compute body length and linear distances traveled. Ground surface temperatures were measured with a copper–constantan thermocouple in contact with the substrate adjacent to the mites' location.

All image processing and remedial motion analysis were performed with Tracker software (Open Source Physics, USA). To calculate speed and acceleration, mite bodies were manually digitized across sequences of 30–100 frames where mites ran in a straight path. Average speeds were also estimated by determining the straight-line distance between the start and end locations of the mites and dividing by the total running period. Within selected trials, the number of contacts between a specific limb tip (usually the second or third limb, depending on visibility) and the ground was divided by the running period to compute the animal's stride frequency f (Hz). The number of individuals used to calculate mean values was different for each type of measurement because the footage from certain trials was not sufficiently clear to determine stride frequency by limb tracking, or because the footage lacked an absolute calibration slide.

Kinematic measures of mites and individual legs during initial acceleration, deceleration and turning were made in the lab in order to obtain sufficient resolution and image quality. Methods followed those described in Wu et al. (2010). Tracker software was used to measure angles of individual legs during the stride cycle relative to the longitudinal axis of the idiosoma in order to calculate stride angles from the beginning to the end of the aerial phase. During the stance phase, we measured the equivalent joint excursions from the time the tarsus contacted the ground surface to the time at which it was lifted. Changes in the orientation of animals during turns were similarly measured by tracking the longitudinal axis of the animal relative to a fixed grid. To compute leg tarsus speeds, the positions of individual leg tarsi in each frame were calculated from the x and y coordinates and distances were tracked between successive frames.

Mites were collected for morphological measurements using an aspirator and preserved in 80% ethanol. M_b of mites was estimated assuming a hemispherical body shape using the following formula:

$$M_b = \rho(V_{sphere}/2), \quad (1)$$

where ρ is density (1 mg mm^{-3} for *P. macropalpis*, following Wu et al., 2010) and V_{sphere} is the volume of a sphere, calculated assuming a mean radius [r=¼×(length+diameter)], and ignoring the legs. Calibrated frames with sufficiently resolved images were used to measure body lengths and diameters across the mites' idiosomae, yielding a mean estimated M_b of 268±18 µg (N=7 individuals) for adult mites and 107±19 µg (N=14 individuals) for juvenile mites. Body lengths and diameters as well as leg lengths were measured using a dissecting microscope equipped with a calibrated eyepiece reticle.

RESULTS

Running speed and stride frequency

Paratarsotomus macropalpis were field-active only at very high ground temperatures, ranging from 43 to 60°C. Juveniles and adults ran at similar absolute speeds (u) at 47.5 and 52.5°C, with a maximum recorded speed of 0.26 m s^{-1} (Table 1). Relative speeds (v_r) in the field averaged 192.4±2.1 BL s^{-1} (N=32 individuals), with the fastest relative speed being 323 BL s^{-1} for a juvenile mite. Comparing data for 47.5 and 52.5°C, v_r for juveniles was significantly higher than that for adults (P<0.01, N=24). Mites ran with an overall mean stride frequency (f) of 99.7±1.1 Hz (N=19), with a maximum recorded value of 135.0 Hz for a juvenile mite. Pearson correlation analysis showed that stride frequency increased

Table 1. Mean running speed and stride frequency for adult and juvenile mites running freely in the field at different ground temperatures

Ground temperature (°C)	Absolute speed, u (m s^{-1})	Relative speed, v_r (BL s^{-1})	Stride frequency, f (Hz)
47.5	0.140±0.005 (2)	133±4.6 (2)	72±9.5 (2)
52.5	0.156±0.005 (4)	203±5.9 (6)	88±2.3 (5)
	0.170±0.019 (5)	159±8.0 (9)	104±5.0 (5)
57.5	0.175±0.009 (4)	242±10.0 (7)	114±5.0 (5)
	N/A	N/A	N/A
	0.120±0.009 (4)	194±9.2 (6)	110±4.8 (2)

Data for adult mites are shown in the upper row for each temperature, and those for juveniles in the lower row. Values are means±s.e.m. (N). BL, body length.

Journal of Experimental Biology (2016) 219, 676-685 doi:10.1242/jeb.128652

significantly as a function of relative speed (r=0.561, P<0.001, N=19). Log transformation of the two variables yielded the following function:

$$f = 26.8 \times v_r^{0.249}. \quad (2)$$

The exponent of 0.249 is significantly smaller than unity (P<10^{-8}, regression t-test), showing that increases in stride frequency only partially explain the higher relative speeds of juvenile mites.

The overall scaling relationship between relative speed and estimated body mass (kg) for juveniles and adults combined is:

$$v_r = 10.22 \times M_b^{-0.199}. \quad (3)$$

Despite the large differences in v_r, values for u and f did not differ significantly between juvenile and adult mites (P=0.6, P=0.4, respectively). In order to test whether juveniles achieve higher relative speeds with proportionally longer legs (and hence longer stride lengths; Weyand et al., 2000), we analyzed the scaling of leg length (l) against body length for 21 preserved mites ranging in body length from 0.62 to 1.43 mm (Fig. 1). Leg length increased progressively from anterior to posterior; for each of the four leg pairs, leg length increased significantly as a function of body length. The combined data for leg length show the following relationship to body length:

$$l = 1.26 \times \mathrm{BL}^{0.641}. \quad (4)$$

Relative speed and stride frequency both increased approximately linearly with temperature. Linear regression was used to calculate Q_{10} values for relative speeds between 45 and 55°C in adult *P. macropalpis*, which yielded a Q_{10} of 1.7 (P=0.03, N=10 individuals); data for juveniles did not yield a statistically significant Q_{10}. Stride frequencies for juveniles and adults combined increased with a Q_{10} of 1.6 (P=0.04, N=17 individuals).

Froude numbers (Fr) provide a dimensionless measure of speed normalized for body size and were calculated for combined mites at different temperatures using the formula (Alexander, 1982):

$$Fr = u^2/(\boldsymbol{g} \times \mathrm{BL}), \quad (5)$$

where u is absolute running speed (m s^{-1}) and $\boldsymbol{g}$ is gravitational acceleration (9.81 m s^{-2}). Data from Table 1 yielded the following Fr values for the three mean temperatures: 1.56 (47.5°C), 2.03 (52.5°C) and 0.99 (57.5°C).

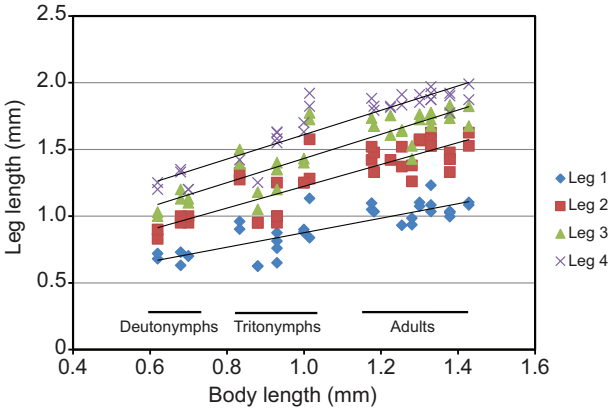

Fig. 1. Measured leg lengths for 21 preserved specimens of *Paratarsotomus macropalpis* as a function of body (idiosoma) length. All four leg pairs scale non-isometrically with body length, with juveniles having proportionally longer legs.

Starting and stopping

Acceleration achieved by mites during starting and stopping was determined by applying a linear regression to the calculated speeds between successive frames (N=10–20 frames per mite). Juvenile and adult mites combined accelerated at an average of 7.2±1.2 m s^{-2} (N=8 individuals) and decelerated at an average of −10.1±2.1 m s^{-2} (N=5 individuals) in the field. Given these mean values, mites will transition between a representative running speed of 0.150 m s^{-1} and rest in 15–20 ms. Values measured in the lab were significantly smaller for both acceleration (2.3±0.76 m s^{-2}, N=5, P<0.002) and deceleration (0.98±0.30 m s^{-2}, N=5, P<0.003). The mean relative force (F/M_b) generated by a representative adult mite (BL=1 mm) during acceleration in the field was 0.52 g.

Braking forces are contributed by air resistance as well as by muscle and elastic elements. We estimated the air resistance for a representative adult mite (BL=1.0 mm, ignoring the legs) running at 0.15 m s^{-1} at 50°C using the formula:

$$F_{drag} = k \times \eta \times \mathrm{BL} \times u, \quad (6)$$

where k is a constant (3π for a spherical mite), η is dynamic viscosity of air (1.98×10^{-5} N s m^{-2} at 50°C), BL is body length (m) and u is absolute velocity (m s^{-1}) (Alexander, 1982). Calculated air resistance (F_{drag}≈2.8×10^{-8} N) is only about 1% of the force required for deceleration (2.5×10^{-6} N) and is therefore insignificant.

By tracking the position of the idiosoma and individual tarsi over time, we were able to analyze limb movements during steady running, as well as during acceleration, deceleration and turning. A representative plot of tarsus speed for the left legs during a straight run is shown in Fig. 2 and the corresponding duty factors are given in Table 2. Opposite limbs move 180 deg out of phase. The near-synchrony of legs 1 and 3 and legs 2 and 4 shows that *P. macropalpis* utilizes an alternating tetrapod gait

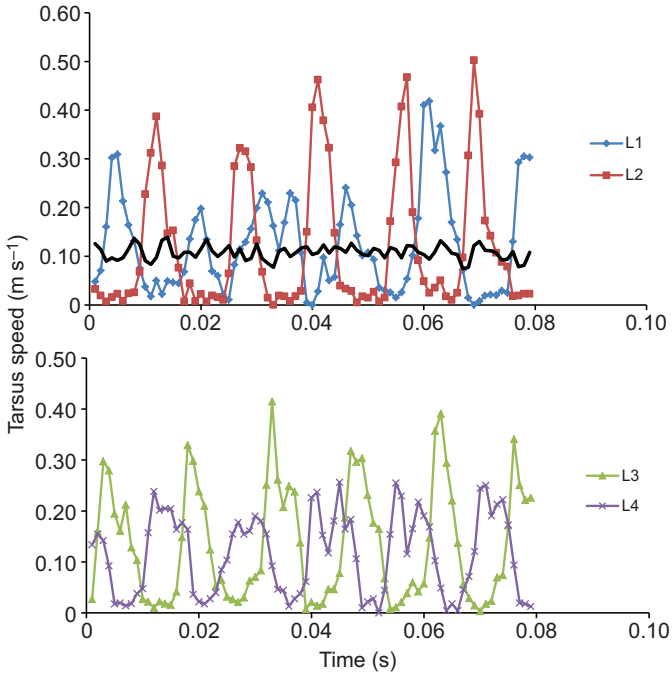

Fig. 2. Tarsal speeds of the four left legs in a representative adult *P. macropalpis* measured during an 80 ms straight run. The upper plot shows data for left (L) legs 1 and 2, with the black line showing the corresponding speed of the body measured at the center of the idiosoma. The lower plot shows data for L3 and L4.

Journal of Experimental Biology (2016) 219, 676-685 doi:10.1242/jeb.128652

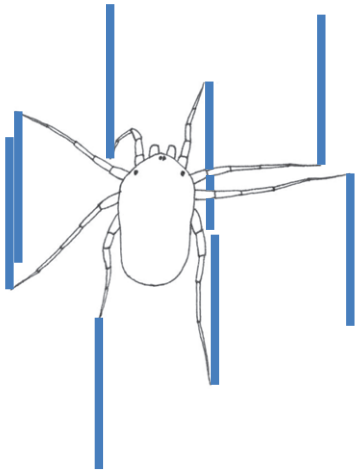

Fig. 3. Gait pattern in *P. macropalpis* sketched from video footage and showing the limbs close to the extremes of the stride excursion. The blue, vertical bars show the approximate longitudinal excursions of each of the eight legs during the previous (R1, R3; L2, L4) and next (R2, R4; L1, L3) aerial phase. Opposite limbs are approximately 180 deg out of phase.

(L1R2L3R4 – L2R1L4R3, etc., where L is left and R is right). No other gait was observed during steady running. Legs 2 and 3 swing in a wide lateral arc. In contrast, the first and fourth leg pairs articulate in the sagittal plane and generate propulsive force by flexion and extension, respectively. The fourth pair of legs is the longest, approximately 1.8 times longer than the first pair, but displayed the lowest tip speeds and longest aerial phase (and hence lowest duty factor) of any of the leg pairs. Their aerial phase typically extended slightly beyond that of the second pair. Changes in speed of the idiosoma were small and did not show an obvious pattern, although a small acceleration was sometimes observed

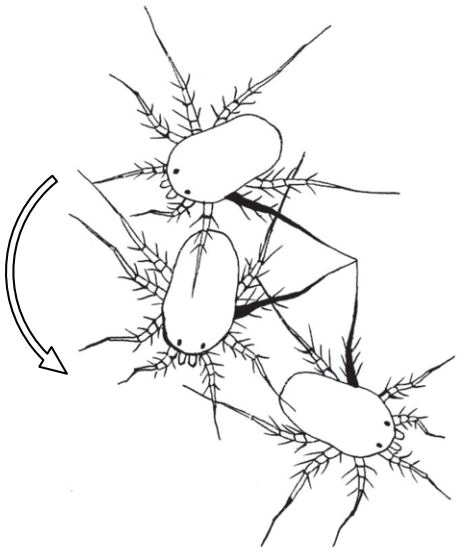

Fig. 4. Diagram of *P. macropalpis* executing a tight left turn through 120 deg while pivoting about L3. The three images are sketched from individual frames of video footage and are separated in time by approximately 60 ms. L3 is shown in black. Most of the long setae on the legs are omitted for clarity. Although the illustration only shows three positions of the mite, this turn encompassed 3.5 gait cycles. The arrow shows the direction of the turn and a scale length of 2 mm.

Table 2. Duty factors for the four leg pairs taken from a representative straight run comprising six stride cycles and including the left leg footage shown in Fig. 2

	1	2	3	4
Duty factor	0.423±0.043	0.426±0.043	0.497±0.017	0.316±0.022
N	10	10	10	10

Values are means±s.e.m.

following the onset of the stationary phase, resulting in an oscillation at twice the period of the gait cycle.

Although air resistance makes a minimal contribution to deceleration of the whole animal, it may represent a significant force slowing the legs during the aerial phase. To determine the drag force acting on the leg during the aerial (recovery) stroke, we modeled it as three cylinders of diminishing diameter (see Appendix). The drag behavior of a cylinder for a range of Reynolds numbers (*Re*) is given in White (2011). For our system, *Re* varies from 0.23 to 0.37 for which drag per unit length (F') is approximated as (Tomotika and Aoi, 1951):

$$F' = \frac{C_D \times \rho \times u_l^2 \times \phi}{2}, \quad (7)$$

where C_D is the drag coefficient in air, ρ is the density of air, u_l is leg velocity and ϕ is leg diameter. This results in a calculated drag force of 1.1×10^{-7} N.

The force required to arrest the leg during deceleration in the recovery stroke can be estimated from the measured deceleration approximated from Fig. 2 (120 m s^{-2}) and an estimated leg mass of 1.9×10^{-9} g. This gives a requisite deceleration force of 2.3×10^{-7} N. The estimated drag force is approximately 40% of the force required to explain the observed deceleration. Taking account of the rather

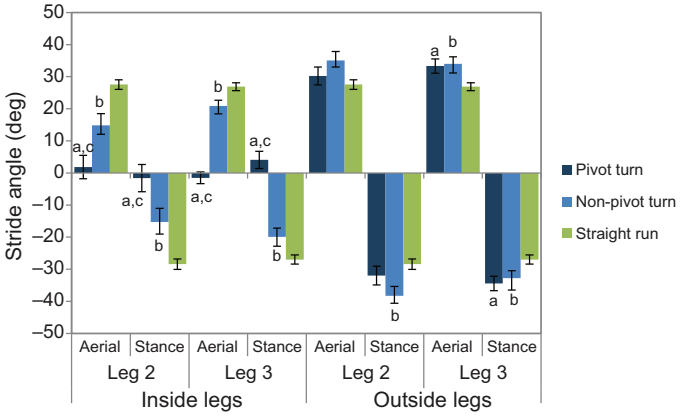

Fig. 5. Stride angles of leg 2 and leg 3 for the aerial (recovery) and stance (active) stroke during pivot turns, non-pivot turns and straight running. Bars show means±1 s.e.m. Inside (ipsilateral) and outside (contralateral) angles for a given leg are the same in the straight runs. Because the inside leg 3 remains in stance during a pivot turn, there was no aerial phase; the angle shown is the equivalent angular change (joint excursion) measured during the recovery stroke. The inside leg 2 and leg 3 remained at similar angles relative to the body during pivot turns while outside stride angles increased relative to a straight run. Non-pivot turns involved an increase in stride angle of the outside leg 2 and leg 3, and a decrease in the equivalent inside stride angles, relative to a straight run, but preserved the basic gait pattern. Means were derived from analysis of five adult mites in each case, using 2–6 gait cycles per animal. Letters denote significant differences (P<0.05) using a 2-way ANOVA to compare stride angles during pivot turns and straight runs (a), non-pivot turns and straight runs (b), and pivot and non-pivot turns (c). N=11–21 for turns and 28–38 for straight runs.

Journal of Experimental Biology (2016) 219, 676-685 doi:10.1242/jeb.128652

Table 3. Summary kinematic data for mites filmed in the lab while using two different modes of turning

Turn type	Body length (mm)	Turning radius (mm)	Turning radius (BL)	Turn angle per gait cycle (deg)	Stride frequency (Hz)	Time per gait cycle (ms)	Angular velocity (deg s^{-1})
Pivot (*N*=11)	1.14±0.03	1.73±0.05	1.53±0.03	30.9±1.31	26.5±2.57	41.5±3.68	795±64
Non-pivot (*N*=8)	1.06±0.05	2.98±0.31	2.84±0.27	25.9±1.61	22.4±3.55	50.8±6.14	567±79
Student's *t*	n.s.	3.99**	–	2.39*	0.92 (n.s.)	1.28 (n.s.)	2.24*

Values are means±s.e.m.
Student's *t* statistics from tests comparing the pivot and non-pivot means are given for each parameter (*P<0.05, **P<0.005).

low stride frequency for the animal in Fig. 2 (67 Hz), these calculations indicate that aerial drag acting on the leg during the recovery stroke is significant, and possibly the primary force arresting the leg at faster running speeds.

The distance covered per stride cycle was calculated from the ratio of running speed to stride frequency (u/f). Based on the mean values measured for adult mites at 52°C (Table 1), the approximate distance per cycle is 1.64 mm. Assuming a symmetrical gait, this will be equal to the average stride length per leg (Fig. 3).

Turning

Mites executed two distinct types of turns: pivoting and non-pivoting. Pivot turns involved a highly stereotypical gait in which the animal pivoted around the tarsus of the inside (ipsilateral) leg 3, which thus functioned like a grappling hook (Fig. 4; Movie 1). Non-pivot turns involved slower angular rotations and were accomplished by reductions in ipsilateral stride angles and proportional increases in contralateral stride angles (Table 3). Mites frequently turned through large angles when utilizing both types of turn; the mean changes in orientation for the turns analyzed were 103.4±48.8 deg (mean±s.d.) for pivots and 102.0±38.6 deg for non-pivots (Table 3). The turning radius in pivot turns (1.73±0.05 mm) was narrowly defined, approximating the length of leg 3 (1.71±0.023 mm), and significantly smaller than for non-pivot turns (2.99±0.31 mm, P<0.05; Table 3). In accordance with their smaller turning radii, pivot turns had higher angular velocities (ω=795±64 deg s^{-1}) when compared with non-pivot turns (567±79 deg s^{-1}, P<0.05). The highest angular velocity measured during a pivot turn was 1253 deg s^{-1} and the highest during a non-pivot turn was 1040 deg s^{-1}. Pivot and non-pivot turns did not differ in stride frequency or angular rotation per gait cycle (Table 3). Pivot and non-pivot turns also did not show any significant difference in stride frequency when compared with straight-running animals (N=8) over a similar temperature range (P>0.1).

Joint excursions for inner legs 2 and 3 during pivot turns were negligible compared with the joint excursions for the outer legs 2 and 3 during pivot turns, non-pivot turns and straight running (Fig. 5). In pivot turns, the joint excursion for the ipsilateral legs was sharply reduced and not significantly different from zero; legs thus maintain a similar angle with respect to the idiosoma while the animal turns. Contralateral legs showed large joint excursions, and in leg 3 these were significantly larger than during straight running. During non-pivot turns, mites preserved the normal alternating tetrapod stepping pattern, but showed a significant reduction in stride angle in the ipsilateral legs, and a corresponding increase in the contralateral stride angle, relative to a straight run.

The footfall patterns of a running mite, starting from rest and executing several turns, illustrate the alternating tripod gait used during straight running and the pivots about L3 during turning (Fig. 6). During initial acceleration (0–0.12 s), animals typically pulled with the first two leg pairs (R2 was not used in the footage used to derive Fig. 6), while legs 3 and 4 dragged passively behind for 3–5 gait cycles. No changes in footfall pattern were discernible during deceleration. Footfall patterns show clearly how animals rotated about the ipsilateral leg 3 when executing a pivot turn; three such turns are included in Fig. 6. While pivoting around the tarsus of leg 3, the duty factor of the ipsilateral leg 2 was reduced. Because of the respective decrease and increase in ipsilateral and contralateral stride lengths, the limb tip speeds differed markedly, but duty factors of legs other than leg 3 and leg 2 changed minimally.

Interspecific scaling of v_r and f

To assess whether v_r in *P. macropalpis* is predicted from interspecific scaling, we examined v_r for fast runners including arachnids (Spagna and Peattie, 2012), mammals (Iriarte-Díaz, 2002) and several other taxa, ranging in size over 10 orders of magnitude (Fig. 7, Table S1). Species were selected to comprise only fast

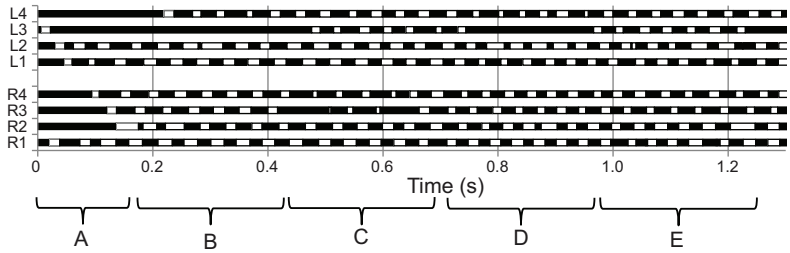

Fig. 6. Footfall diagram for a representative *P. macropalpis* accelerating from rest followed by a period of running and turning in the lab. Each horizontal bar depicts the footfall pattern of a single limb with black showing the stance (ground) phase and white showing the swing (aerial) phase. Bracketed periods A–E denote specific locomotory patterns. (A) Initial acceleration: the mite pulls at the ground with the first two leg pairs. The rear two pairs are dragged briefly before adopting the alternating tetrapod gait cycle. (B) Left turn, pivoting around L3. The gait cycle is essentially preserved, but stride length is reduced in L2 to enable the turn. (C) Right turn, pivoting about R3. Contact between R3 and the ground is broken briefly several times, resulting in a shallower turn. (D) Left turn pivoting about L3. (E) Straight run showing the stereotypical alternating tetrapod gait cycle.

Journal of Experimental Biology

Journal of Experimental Biology (2016) 219, 676-685 doi:10.1242/jeb.128652

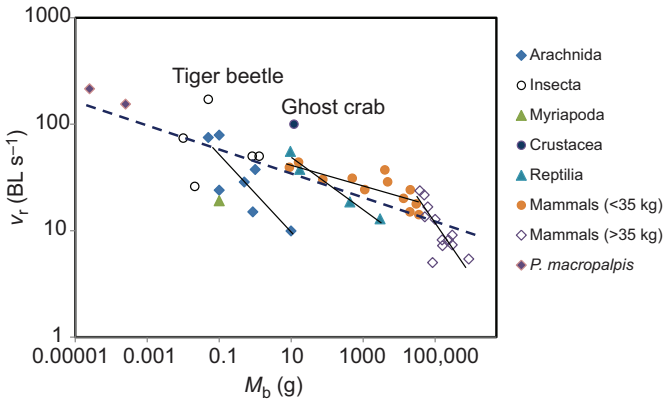

Fig. 7. Relative speed (v_r) of adult and juvenile *P. macropalpis* running in the field as a function of body mass (M_b) compared with published data for other running animals. Least-squares regression lines are shown for arachnids (β=−0.34), reptiles (β=−0.24), mammals <35 kg (β=−0.099) and mammals >35 kg (β=−0.42). The dashed line shows the least-squares regression for the combined data (β=−0.112). A list of species included here, with references, is given in Table S1.

runners (typically cursorial or ambush predators with high sprint speed), and drawn from as wide an array of taxa as possible, minimizing over-representation of specific families. Thus, we included data for two of the fastest ants, despite data being available for multiple ant species (e.g. Hurlbert et al., 2008). The mean BL of juvenile mites filmed in the field on all calibrated footage was 711±43 µm (N=14 individuals), and the mean BL for adults was 1005±23 µm (N=7 individuals).

Mite speeds are closely predicted by scaling for the combined data (β=−0.112, or −0.103 when *P. macropalpis* is excluded) and by a regression for running arthropods excluding *P. macropalpis* (β=−0.104), where β is the scaling exponent for v_r against M_b.

DISCUSSION

The mean relative speed of 192.4 BL s^{-1} measured for *P. macropalpis* in this study is the highest value for v_r currently documented for any terrestrial animal, exceeding the highest previously published value of 171 BL s^{-1} for the Australian tiger beetle, *Cicindela eburneola* (Kamoun and Hogenhout, 1996). The maximum stride frequency reported here, 135 Hz, is also the highest reported value for any weight-bearing muscle. The faster speeds relative to the lab measurements reported for this species by Wu et al. (2010) may be attributable in part to poor traction on the enamel substrate used for lab trials, but we believe they are also likely to be explained by injury sustained by animals during collection. Animals collected with an aspirator frequently had damaged legs and impaired mobility.

Juvenile *P. macropalpis* run at similar absolute speeds to adult mites, but consequently attain significantly higher relative speeds (Table 1). Comparing juveniles and adults, differences in stride frequency only partly explain the higher v_r in juveniles ($f \propto v_r^{0.249}$, Eqn 2). The requisite differences in stride length are consistent with the proportionally longer legs of juveniles (Eqn 3). This ontogenetic change in relative stride length allows the smaller juveniles to run at similar absolute speeds to adults (Fig. 1). Adults and juveniles show similar Froude numbers, ranging from 0.99 to 2.03 depending on temperature, and conforming broadly to values published for other running arthropods (Biewener, 2003; Full, 2011) and for symmetrical gaits in tetrapods, consistent with the dynamic similarity hypothesis (Alexander and Jayes, 1983). To put this in context, running mammals and lizards typically transition to asymmetric gaits at Froude numbers between 2 and 3.

Because mites were only field-active over a limited temperature range (substrate temperatures of 43–60°C), we had a smaller temperature range from which to assess the effect of temperature on running speed and stride frequency than in the lab trials used by Wu et al. (2010). However, our Q_{10} values for v_r (1.70) and f (1.60) calculated over 45–55°C show good agreement with the respective lab values for u (1.61) and f (1.59) calculated by Wu et al. (2010) for 40–50°C. Interestingly, neither u nor f showed the steep declines above 50°C reported by Wu et al. (2010). This decline in running performance in the prior study may be attributable to stress or injury sustained during field collection, but could also be a consequence of the rapid heating and cooling (between 22°C and experimental temperatures) imposed by the lab trials. Either way, while animals running freely in the field show a plateau and perhaps a modest decline in running performance above 55°C (Table 1), they are clearly able to maintain exceptional speeds at temperatures up to 60°C. Indeed, our second highest measured relative speed (301 BL s^{-1}) was for a juvenile at 60°C.

Despite the extremely high relative speeds and stride frequencies attained by *P. macropalpis*, allometric comparisons with other fast-running animals do not show the mite to be an outlier. The exceptional relative speeds documented for the tiger beetle *Cicindella eburneola* (Kamoun and Hogenhout, 1996) and the ghost crab *Ocypode ceratophthalma* (Burrows and Hoyle, 1973) present as much more dramatic outliers (Fig. 7; Table S1). Relative speeds (present study) and stride frequencies (Wu et al., 2010) for *P. macropalpis* are well predicted by interspecific scaling. The scaling exponent of −0.112 derived from our interspecific comparison underestimates mite v_r slightly, but almost exactly predicts mite speeds if these are adjusted using our Q_{10} values for a more representative temperature of 40°C (yielding v_r values of approximately 110 BL s^{-1}). Comparative data for arthropods yield a similar scaling exponent for v_r against M_b (−0.104). Taken together, allometric comparisons support the dynamic similarity of *P. macropalpis* to other running animals. Caution should be applied, however, given the paucity of arthropod data, particularly for myriapods and crustaceans. More information is available for other arachnid orders (Spagna and Peattie, 2012), and these appear to show a steeper scaling of v_r with M_b, but as with other arthropods the data show considerable variance and lack representative species for several orders. Terrestrial runners are restricted to two major taxa – tetrapods and arthropods – with little overlap in mass ranges, which presents challenges to the application of phylogenetic comparative methods (Felsenstein, 1985; Garland et al., 2005; see also Rohlf, 2006). Future analyses accounting for independent origins of a running habit, and independent land colonization by different arthropod subphyla, may help to inform our understanding of v_r scaling.

Paratarsotomus macropalpis employs an alternating tetrapod gait as seen also in spiders (Ward and Humphreys, 1981; Biancardi et al., 2011) and several other arachnid orders (Spagna and Peattie, 2012). Although temporal resolution in our footage is limited by the very high stride frequencies (ca. 10 frames per stride cycle), duty factors approximate 0.5 for leg 3, 0.42 for leg 1 and leg 2, and somewhat lower (0.32) for leg 4. This pattern is modified during acceleration, when the third and fourth leg pairs are dragged passively for 2–5 gait cycles. Based on our measurements of initial acceleration in the field and in the lab, this corresponds to the time required to attain a steady running speed (20–60 ms).

Journal of Experimental Biology (2016) 219, 676-685 doi:10.1242/jeb.128652

When executing tight turns, mites show a stereotypical gait, pivoting around the tarsus of the ipsilateral third leg. Such turns appear to involve the tarsus functioning as a grapple. The flexible distal part of the leg can be seen to stretch taut intermittently as the mite pivots, consistent with the anchor of the tarsal claws serving in the transfer of angular momentum (see Movie 1). In a shallow right turn, R3 follows the usual gait cycle but with reduced stride length and an increased duty factor, and may skip the aerial phase in adjacent gait cycles. Both pivot and non-pivot turns may involve very high angular velocities. The mean value for ω during pivot turns in the lab was 795±64 deg s^{-1}, which likely underestimates angular velocities at the higher stride frequencies exhibited in field conditions. Given the mites' ability to turn through 180 deg in 6–7 gait cycles, and assuming a stride frequency in the field of 100 Hz, they would be able to accomplish such a turn in less than 0.1 s. The peak angular velocity achieved by a pivoting mite in the current lab trials exceeded 1250 deg s^{-1}. This pivoting, lateral turn by the mite is comparable in angular velocity to the inversion behavior seen in the cockroach *Periplaneta*, which uses a similar grappling hook mechanism to pivot vertically around the tarsus of a limb during escape (>1200 deg s^{-1}; Mongeau et al., 2012). Unlike *Periplaneta*, however, the mites continued to cycle their other limbs to move through the turn about the pivoted leg (Fig. 4, Table 3).

Although the pivoting (or grappling hook) mechanism has been described in inverting cockroaches and geckos (Mongeau et al., 2012), this use of a grappling hook during turning in *P. macropalpis* differs substantially from that described for most other arthropods. The octopodal gait in the tarantula *Grammostola mollicoma* uses a gait cycle where the ipsilateral legs are reversed during a sharp turn (Biancardi et al., 2011). Honey bees and dung beetles use similar ipsilateral gait reversals during tight turns (Zolotov et al., 1975; Frantsevich and Mokrushov, 1980). During more shallow turns, honey bees utilize similar gait adjustments to *P. macropalpis*, pivoting around the ipsilateral hind leg or relying on adjustments in stride length as the turning radius increases (Zolotov et al., 1975). During tight turns on a stick, squash bugs and stick insects also sometimes pivot slowly about the ipsilateral hind leg (Frantsevich and Cruse, 2005; Cruse et al., 2009). Other than for the ipsilateral leg 2 and leg 3, stride frequency and duty factor do not change markedly during turning in *P. macropalpis* (Fig. 5), which is consistent with leg kinematics during turning in the spider *Metaphidippus hartfordi* (Land, 1972). Similar preservation of stride frequency and duty factor during turning is typical also for hexapods – for example, the fruit fly *Drosophila melanogaster* (Strauß and Heisenberg, 1990), 12 species of ants (Zollikofer, 1994) and the large cockroach *Blaberus discoidalis* (Jindrich and Full, 1999).

Mites, like several other arachnid orders, appear to lack leg extensor muscles in many or all of the joints and to depend on a threshold hemocoelic pressure to maintain leg extension (Shultz, 1989). This is apparent in *P. macropalpis* from the way in which the legs fold ventrally when animals are quiescent or dead, in a similar manner to those of spiders. Hydraulic leg extension, well documented in spiders and other larger arachnids (Parry and Brown, 1959; Alexander, 1967; Shultz, 1991), is unlikely in *P. macropalpis* because the viscosity of hemocoelic fluid would not allow for movement in/out of the legs' narrow hemolymph canals at the rates required to sustain measured stride frequencies (Sensenig and Shultz, 2003). The measured lumen diameter of the basifemur, telofemur and patella in the legs of an adult *P. macropalpis* is 40–60 µm. Assuming the viscous drag of hydraulic fluid follows Poiseuille's law (drag$\propto r^{-4}$), *P. macropalpis* legs would have about 10^7 times the viscous drag of legs in a large arachnid such as *Aphonopelma*. Instead, it is probable that mites extend the main leg joints using the release of energy stored in loaded elastic sclerites (Sensenig and Shultz, 2003). Eliminating extensor muscles would confer the benefit of reducing leg mass and inertia and hence the kinetic energy required to sustain high stride frequencies (Full and Tu, 1991). Interestingly, there are only minor differences discernible in the kinetics of leg movements despite the fact that the active and recovery leg strokes likely employ fundamentally different mechanisms in the different leg pairs. Thus, in the extreme case, the first leg pair employs muscular shortening to flex the limb elements during the active stroke, which pulls the animal forward. By contrast, in the fourth leg pair, the active stroke (stance phase) involves leg extension and probably employs the release of energy from loaded elastic sclerites, while muscle shortening flexes the limb during the recovery stroke. The storage and release of elastic energy in leg sclerites is clearly able to operate at the extreme frequencies (up to 135 Hz) observed. However, the reduced duty factor seen in the fourth legs, and the fact that the third and fourth pairs of legs are dragged passively during initial acceleration while the anterior legs pull the animal forward, may suggest that leg extension using elastic sclerites generates low propulsive force relative to muscular flexion.

During deceleration, mites did not show any clear change in gait pattern. As air resistance is insufficient to explain observed deceleration, the main reaction forces employed in slowing are again probably imparted by the loading of elastic sclerites between the limb elements. At the cessation of the gait cycle on stopping, the idiosoma could be seen to rise and swing forward, representing the final transfer of forward momentum. A probable related function of elastic sclerites in *P. macropalpis* is passive energy absorption and dissipation (Sensenig and Shultz, 2003). Although we filmed animals on a concrete driveway, the species also occurs locally on open ground in coastal sage scrub habitats (Wu et al., 2010). The soils here comprise finely sorted alluvial sands and gravels and represent a very uneven terrain to an animal of ca. 1 mm. Passive shock-absorption of elastic elements may confer an important role in both stability and energy conservation, countering the constant shifting of a mite's center of mass when running on a typical substrate.

Measured values for acceleration and deceleration in *P. macropalpis*, although appearing very rapid, are comparable to values published for other running animals. Hunting cheetahs achieve accelerations between 0.1 and 1.0 $\boldsymbol{g}$ (Wilson et al., 2013), and the maximum acceleration achieved by Usain Bolt in the 100 m dash is 0.97 $\boldsymbol{g}$ (Hernández Gómez et al., 2013). These similarities are consistent with the prediction that muscle work scales in proportion to muscle mass and body mass, allowing animals of different masses to attain comparable acceleration (Hill, 1950; Alexander, 1982).

Notwithstanding the exceptional relative speed and stride frequency shown by *P. macropalpis*, the good prediction of v_r and f from interspecific scaling (Fig. 7; Wu et al., 2010) indicates that the muscle contraction frequencies are likely optimized to exploit limb resonance for energy efficiency and are not limited by the force–velocity trade-off (Full, 2011). Because muscle force scales in proportion to cross-sectional area ($\propto M^{0.67}$), the relative muscle force per unit mass (F/M) scales as $M^{-0.33}$ ($M^{0.67}/M^{1}$), increasing as animals get smaller. Just as large animals need disproportionately large leg muscles to support their weight, very small animals can

Journal of Experimental Biology (2016) 219, 676-685 doi:10.1242/jeb.128652

sacrifice muscle mass or the relative volume of myofibrils within a fiber. Even though *P. macropalpis* exhibits superfast weight-bearing muscles, the relative force they must generate is small by virtue of the mite's small mass. A larger portion of the mite's muscle volume could therefore be allocated to the mitochondria and SR as in other ultra-fast (non-weight-bearing) muscles such as rattlesnake tail shaker muscles (Schaeffer et al., 1996) or the sonic swim bladder muscles in toadfish (Appelt et al., 1991; Rome et al., 1996). An open question is whether the predicted increase in stride frequency and relative speed for even smaller animals is ultimately limited by excitation–contraction coupling, calcium cycling or other components of muscle performance. The fact that direct weight-bearing muscles can achieve the stride frequencies measured in juvenile mites (up to 135 Hz), involving contraction and relaxation times not exceeding 4 ms, demonstrates the extraordinary plasticity of muscle physiology.

In summary, *Paratarsotomus macropalpis* exhibits several exceptional locomotory attributes. In addition to attaining the fastest relative speed and stride frequency documented for running animals, the mites are capable of turning with extremely high angular velocities by utilizing the ipsilateral leg 3 as a grappling hook. Allometric scaling of leg length during development results in proportionally longer legs in juveniles and allows them to attain absolute and relative speeds comparable to those of adults.

Appendix

The following analysis explains the calculation of the aerial drag force acting on the mite legs during the recovery stroke. The drag force acting on leg 2 and leg 3 was estimated assuming a mean leg velocity (u_l) of 0.4 m s^{-1} (see Fig. 2), and leg length of 1.7 mm, approximating the leg as three cylinders with length (l) and diameter (ϕ) as shown in Fig. A1.

Leg segment lengths and diameters were measured in alcohol-preserved specimens. Diameters varied from approximately 0.06 mm at the basifemur to 0.03 mm at the tibia and 0.02 mm at the tarsus. The cylinders here were modeled to approximate the dimensions of the combined basifemur, telofemur and patella (1), tibia (2) and tarsus (3).

The drag coefficient (C_D) was calculated for each of the cylinders (1, 2, 3) using the following solution for the Oseen equation (Tomotika and Aoi, 1951):

$$\begin{aligned} C_D &= 2F'/\rho \times u_l^2 \times \phi \\ &= 8\pi/Re[0.5 - \Gamma + \ln(8/Re)], \end{aligned} \quad \text{(A1)}$$

where F' is the force per unit length on the cylinder, ρ is the density of air (1.086 kg m^{-3}), Re is the Reynolds number and Γ is Euler's constant (0.577). $Re=\phi\times u_l/\nu$, where ν is the kinematic viscosity of air at 325 K (=1.807×10^{-5} m^2 s^{-1}); hence, for the cylinders:

$$\begin{aligned} Re_1 &= [(5 \times 10^{-5}\ \text{m})(0.4\ \text{m s}^{-1})(0.35/1.70\ \text{mm})]/ \\ &\quad (1.807 \times 10^{-5}\ \text{m}^2\ \text{s}^{-1}) = 0.23, \\ Re_2 &= Re_1(0.92\ \text{mm}/0.35\ \text{mm})(0.03\ \text{mm}/0.05\ \text{mm}) = 0.36, \\ Re_3 &= Re_1(1.425\ \text{mm}/0.35\ \text{mm})(0.02\ \text{mm}/0.05\ \text{mm}) = 0.37. \end{aligned}$$

Applying these values to Eqn 3 yields the following dimensionless drag coefficient (C_D) estimates for segments 1–3, respectively: 32, 23 and 23. Rearranging Eqn 3:

$$F' = C_D \times \rho \times u_l^2 \times \phi/2. \quad \text{(A2)}$$

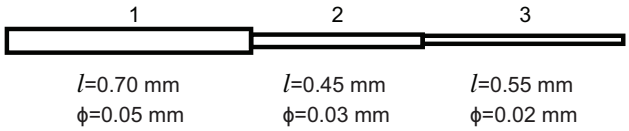

Fig. A1. Approximation of the leg as three cylinders. l, leg segment length; ϕ, leg segment diameter.

The drag force (F_i, where i represents the segment) acting on each division of the leg can then be calculated, and summed to yield an estimate of drag force F_{total} for the whole leg:

$$\begin{aligned} F'_1 &= [(32\ \text{N m}^{-1})(1086\ \text{kg m}^{-3})(0.08\ \text{m s}^{-1})^2(5 \times 10^{-5}\ \text{m})]/2 \\ &= 6.9 \times 10^{-5}\ \text{N m}^{-1}, \\ F_1 &= (6.9 \times 10^{-5})(7 \times 10^{-4}\ \text{m}) \\ &= 4.9 \times 10^{-8}\ \text{N}, \end{aligned} \quad \text{(A3)}$$

$$\begin{aligned} F'_2 &= [(23\ \text{N m}^{-1})(1086\ \text{kg m}^{-3})((0.4\ \text{m s}^{-1})(0.92/1.7))^2 \\ &\quad (2.5 \times 10^{-5}\ \text{m})]/2 \\ &= 4.4 \times 10^{-5}\ \text{N m}^{-1}, \\ F_2 &= (4.4 \times 10^{-5})(4.5 \times 10^{-4}\ \text{m}) \\ &= 2.0 \times 10^{-8}\ \text{N}, \end{aligned} \quad \text{(A4)}$$

$$\begin{aligned} F'_3 &= [(23\ \text{N m}^{-1})(1086\ \text{kg m}^{-3})((0.4\ \text{m s}^{-1})(1.425/1.7))^2 \\ &\quad (2 \times 10^{-5}\ \text{m})]/2 \\ F_3 &= (7.0 \times 10^{-5})(5.5 \times 10^{-4}\ \text{m}) \\ &= 3.9 \times 10^{-8}\ \text{N}, \end{aligned} \quad \text{(A5)}$$

$$\begin{aligned} F_{\text{total}} &= (4.9 + 2.0 + 3.9) \times 10^{-8} \\ &= 1.1 \times 10^{-7}\ \text{N}. \end{aligned} \quad \text{(A6)}$$

The force required to arrest the leg can be estimated using the measured deceleration of leg 2 and leg 3 (ca. 120 m s^{-2}; Fig. 2) and by estimating the leg mass as $\sum\pi(\phi/2)^2\times l\times\rho_l$ for the three cylinders, where l is cylinder length and ρ_l is leg density (estimated at 1100 kg m^{-3}):

$$\begin{aligned} &\text{Required deceleration force} = \\ &\quad 120\,(1100 \times 10^3)[\pi(2.5 \times 10^{-5}\ \text{m})^2(7 \times 10^{-4}\ \text{m})] \\ &\quad + [\pi(1.5 \times 10^{-5}\ \text{m})^2(4.5 \times 10^{-4}\ \text{m})] \\ &\quad + [\pi(1 \times 10^{-5}\ \text{m})^2(5.5 \times 10^{-4}\ \text{m})] \\ &\quad = 2.5 \times 10^{-7}\ \text{m s}^{-2}. \end{aligned} \quad \text{(A7)}$$

Acknowledgements

The authors thank Ivo Ros for helpful discussions on data collection and software troubleshooting, as well as Jeremy Wright for his assistance with mite collection and filming. We are grateful to the feedback of two anonymous reviewers, including the suggestion to examine the role of air drag in slowing legs during the aerial phase. We thank the Departments of Biology and Physics at Pomona College, the Department of Biology at Harvey Mudd College, and the Keck Science Department.

Competing interests
The authors declare no competing or financial interests.

Author contributions
S.R. and M.H.-Y.Y. performed experiments and all authors collaborated in data analysis. S.R. and J.C.W. prepared the manuscript. J.C.W., D.L.W. and A.N.A. advised and oversaw the entire research endeavor and also helped to revise the manuscript prior to submission.

Funding
This study was conducted with the support of the Howard Hughes Medical Institute Undergraduate Science Program awards 52006301 to Harvey Mudd College and 52007544 to the Claremont Colleges.

Supplementary information
Supplementary information available online at
http://jeb.biologists.org/lookup/suppl/doi:10.1242/jeb.128652/-/DC1

References

Alexander, R. M. (1967). Problems of limb extension in the scorpion, *Opisthophthalmus latimanus* Koch. *Trans. R. Soc. S. Afr.* **37**, 165-181.
Alexander, R. M. (1982). *Locomotion of Animals*. Bishopbriggs, Glasgow: Blackie & Son Limited.
Alexander, R. M. and Jayes, A. S. (1983). A dynamic similarity hypothesis for the gaits of quadrupedal mammals. *J. Zool.* **201**, 135-152.
Amaya, C. C., Klawinski, P. D. and Formanowicz, D. R., Jr (2001). The effects of leg autotomy on running speed and foraging ability in two species of wolf spider, (Lycosidae). *Am. Mid. Nat.* **145**, 201-205.
Appelt, D., Shen, V. and Franzini-Armstrong, C. (1991). Quantitation of Ca ATPase, feet and mitochondria in superfast muscle fibres from the toadfish, *Opsanus tau*. *J. Muscle Res. Cell Motil.* **12**, 543-552.
Banks, N. (1916). New Californian mites. *Calif. J. Entomol. Zool.* **8**, 12-16.
Biancardi, C. M., Fabrica, C. G., Polero, P., Loss, J. F. and Minetti, A. E. (2011). Biomechanics of octopedal locomotion: kinematic and kinetic analysis of the spider *Grammostola mollicoma*. *J. Exp. Biol.* **214**, 3433-3442.
Biewener, A. A. (2003). *Animal Locomotion*. New York, NY: Oxford University Press.
Burrows, M. and Hoyle, G. (1973). The mechanism of rapid running in the ghost crab *Ocypode ceratophthalma*. *J. Exp. Biol.* **58**, 327-349.
Clemente, C. J., Thompson, G. G. and Withers, P. C. (2009). Evolutionary relationships of sprint speed in Australian varanid lizards. *J. Zool.* **278**, 270-280.
Cruse, H., Ehmanns, I., Stübner, S. and Schmitz, J. (2009). Tight turns in stick insects. *J. Comp. Physiol. A* **195**, 299-309.
Felsenstein, J. (1985). Phylogenies and the comparative method. *Am. Nat.* **125**, 1-15.
Foellmer, M. W., Marson, M. and Moya-Laraño, J. (2011). Running performance as a function of body size, leg length and angle of incline in male orb-web spiders *Argiope aurantica*. *Evol. Ecol. Res.* **13**, 513-526.
Frantsevich, L. I. and Cruse, H. (2005). Leg coordination during turning on an extremely narrow substrate in a bug, *Mesocerus marginatus* (Heteroptera, Coreidae). *J. Insect Physiol.* **51**, 1092-1104.
Frantsevich, L. I. and Mokrushov, P. A. (1980). Turning and righting in Geotrupes (Coleoptera, Scarabaeidae). *J. Comp. Physiol.* **136**, 279-289.
Full, R. J. (2011). Invertebrate locomotor systems. *Compr. Physiol.* **30**, 853-930.
Full, R. J. and Tu, M. S. (1991). Mechanics of six-legged runners. *J. Exp. Biol.* **148**, 129-146.
Garland, T. (1983). The relation between maximal running speed and body mass in terrestrial mammals. *J. Zool.* **199**, 157-170.
Garland, T., Bennett, A. F. and Rezende, E. L. (2005). Phylogenetic approaches in comparative physiology. *J. Exp. Biol.* **208**, 3015-3035.
Gorb, S. N. and Barth, F. G. (1994). Locomotion behavior during prey capture of a fishing spider *Dolomedes plantarius* (Aranae: Araneidae): galloping and stopping. *J. Arachnol.* **22**, 89-93.
Hernández Gómez, J. J., Marquina, V. and Gómez, R. W. (2013). On the performance of Usain Bolt in the 100 m sprint. *Eur. J. Phys.* **34**, 1227-1233.
Hill, A. V. (1950). The dimensions of animals and their muscular dynamics. *Sci. Prog. Lond.* **38**, 209-230.
Hurlbert, A. H., Ballantyne, F. and Powell, S. (2008). Shaking a leg and hot to trot: the effects of body size and temperature on running speed in ants. *Ecol. Entomol.* **33**, 144-154.
Iriarte-Díaz, J. (2002). Differential scaling of locomotor performance in small and large terrestrial mammals. *J. Exp. Biol.* **205**, 2897-2908.
Irschick, D. J. and Jayne, B. C. (1999). Comparative three-dimensional kinematics of the hindlimb for high-speed bipedal and quadrupedal locomotion of lizards. *J. Exp. Biol.* **202**, 1047-1065.
Jindrich, D. L. and Full, R. J. (1999). Many-legged maneuverability: dynamics of turning in hexapods. *J. Exp. Biol.* **202**, 1603-1623.
Jones, J. H. and Lindstedt, S. L. (1993). Limits to maximal performance. *Ann. Rev. Physiol.* **55**, 547-569.
Kamoun, S. and Hogenhout, S. A. (1996). Flightlessness and rapid terrestrial locomotion in tiger beetles of the *Cicindela* L. Subgenus *Rivacindela* van Nidek from saline habitats of Australia (Coleoptera: Cicindelidae). *Coleopt. Bull.* **50**, 221-230.
Land, M. (1972). Stepping patterns made by jumping spiders during turns mediated by the lateral eyes. *J. Exp. Biol.* **56**, 15-40.
Manton, S. M. (1965). The evolution of arthropodan locomotory mechanisms. Part 8. Functional requirements and body design in Chilopoda, together with a comparative account of their skeleto-muscular systems and an Appendix on a comparison between burrowing forces of annelids an. *J. Linn. Soc. Lond. Zool.* **45**, 251-484.
Mongeau, J.-M., McRae, B., Jusufi, A., Birkmeyer, P., Hoover, A. M., Fearing, R. and Full, R. J. (2012). Rapid inversion: running animals and robots swing like a pendulum under ledges. *PLoS ONE* **7**, e38003.
Nicolson, S. W., Bartholemew, G. A. and Seely, M. K. (1984). Ecological correlates of locomotion speed, morphometries and body temperature in three Namib Desert tenebrionid beetles. *S. Afr. J. Zool.* **19**, 131-134.
Otto, J. C. (2000). A cladistic analysis of Erythracarinae (Acarina: Prostigmata: Anystidae), with the description of a new genus. *Syst. Entomol.* **25**, 447-484.
Parry, D. A. and Brown, R. H. J. (1959). The hydraulic mechanism of the spider leg. *J. Exp. Biol.* **36**, 423-433.
Pennycuick, C. J. (1975). On the running of the gnu (*Connochaetes taurinus*) and other animals. *J. Exp. Biol.* **63**, 775-799.
Punzo, F. (1998). *The Biology of Camel Spiders (Arachnida, Solifugae)*. New York: Springer.
Rohlf, F. J. (2006). A comment on phylogenetic correction. *Evolution* **60**, 1509-1515.
Rome, L. C. (2006). Design and function of superfast muscles: new insights into the physiology of skeletal muscle. *Ann. Rev. Physiol.* **68**, 193-221.
Rome, L. C., Syme, D. A., Hollingworth, S., Lindstedt, S. L. and Baylor, S. M. (1996). The whistle and the rattle: the design of sound producing muscles. *Proc. Nat. Acad. Sci. USA* **93**, 8095-8100.
Schaeffer, P. J., Conley, K. E. and Lindstedt, S. L. (1996). Structural correlates of speed and endurance in skeletal muscle: the rattlesnake tailshaker muscle. *J. Exp. Biol.* **198**, 351-358.
Schmidt-Nielsen, K. (1984). *Why is Animal Size so Important?* Cambridge, UK: Cambridge University Press.
Sensenig, A. T. and Shultz, J. W. (2003). Mechanics of cuticular elastic energy storage in leg joints lacking extensor muscles in arachnids. *J. Exp. Biol.* **206**, 771-784.
Shultz, J. W. (1989). Morphology of locomotor appendages in Arachnida: evolutionary trends and phylogenetic implications. *Zool. J. Linn. Soc.* **97**, 1-55.
Shultz, J. W. (1991). Evolution of locomotion in Arachnida: the hydraulic pressure pump of the giant whipscorpion, *Mastigoproctus giganteus* (Uropygi). *J. Morphol.* **210**, 13-31.
Spagna, J. C. and Peattie, A. M. (2012). Terrestrial locomotion in arachnids. *J. Insect Physiol.* **58**, 599-606.
Spagna, J. C., Valdivia, E. and Mohan, V. (2011). Gait characteristics of two fast-running spider species (*Hololena adnexa* and *Hololena curta*), including an aerial phase (Araneae: Agelenidae). *J. Arachnol.* **39**, 84-91.
Strauß, R. and Heisenberg, M. (1990). Coordination of legs during straight walking and turning in *Drosophila melanogaster*. *J. Comp. Physiol. A* **167**, 403-412.
Tomotika, S. and Aoi, S. (1951). An expansion formula for the drag on a circular cylinder moving through a viscous fluid at small Reynolds numbers. *Q. J. Mech. Appl. Math.* **4**, 401-406.
Ward, T. M. and Humphreys, F. W. (1981). Locomotion in burrowing and vagrant wolf spiders (Licosidae). *J. Exp. Biol.* **92**, 305-321.
Wehner, R. (1983). Taxonomie, Funktionsmorphologie und Zoogeographie der saharischen Wüstenameise *Cataglyphis fortis* (Forel 1902) stat. nov. *Senckenbergiana Biol.* **64**, 89-132.
Weihmann, T. (2013). Crawling at high speeds: steady level locomotion in the spider Cupiennius salei—global kinematics and implications for centre of mass dynamics. *PLoS ONE* **8**, e65788.
Weyand, P. G., Sternlight, D. B., Bellizzi, M. J. and Wright, S. (2000). Faster top running speeds are achieved with greater ground forces not more rapid leg movements. *J. Appl. Physiol.* **89**, 1991-1999.
White, F. M. (2011). *Fluid Dynamics*, 7th edn. New York, NY: McGraw-Hill.
Wilson, A. M., Lowe, J. C., Roskilly, K., Hudson, P. E., Golabek, K. A. and McNutt, J. W. (2013). Locomotion dynamics of hunting in wild cheetahs. *Nature* **498**, 185-189.
Wittlinger, M., Wehner, R. and Wolf, H. (2007). The desert ant odometer: a stride integrator that accounts for stride length and walking speed. *J. Exp. Biol.* **210**, 198-207.
Wu, G. C. and Wright, J. C. (2015). Exceptional thermal tolerance and water resistance in the mite *Paratarsotomus macropalpis* (Erythracaridae)

challenge prevailing explanations of physiological limits. *J. Insect Physiol.* **82**, 1-7.

Wu, G. C., Wright, J. C., Whitaker, D. L. and Ahn, A. N. (2010). Kinematic evidence for superfast locomotory muscle in two species of teneriffiid mites. *J. Exp. Biol.* **213**, 2551-2556.

Zollikofer, C. P. (1994). Stepping patterns in ants. I. Influence of speed and curvature. *J. Exp. Biol.* **192**, 95-106.

Zolotov, V., Frantsevich, L. and Falk, E.-M. (1975). Kinematik der phototaktischen Drehung bei der honigbiene *Apis mellifera* L. *J. Comp. Physiol.* **97**, 339-353.

Movie 1. Pivot turn movie. Footage of *P. macropalpis* executing a pivot turn, initially in real-time and then slowed 1/30.

Table S1. Relative speed and mass data for fast-running animals included in Fig. 7

Species	v_r (BL s^{-1})	M_b (g)	References
Arthropoda			
Arachnida			
Araneae			
Argiope aurantia	15.0	0.86	Foellmer et al., 2011
Dolomedes plantarius	37.5	1	Gorb and Barth, 1994[M]
Hololena adnexa	24	0.1	Spagna et al., 2011[M]
Hololena adnexa	79	0.1	
Eratigena atrica	28.6	0.5	Guinness Book
Schizocosa ocreata	75	0.05	Amaya et al., 2001[L]
Solifugae			
Eremobates marathoni	9.9	9.9	Punzo, 1998
Acari			
Paratarsotomus macropalpis	154	0.00025	Current study
	214.6	0.000025	
Insecta			
Formica polyctena	26	0.021	Hurlbert et al., 2008
Cataglyphis bombycina	74	0.01	Wehner, 1983; Wittlinger et al., 2007
Periplaneta americana	50	0.83	Full and Tu, 1991
Onymacris plana	50	1.3	Nicolson, Bartholemew and Seeley, 1984
Cicindela eburneola	171	0.05	Kamoun and Hogenhout, 1996
Myriapoda - Chilopoda			
Scutigera coleoptrata	19.1	0.1	Manton, 1965
Crustacea			
Ocypode centrophthalma	100	12	Burrows and Hoyle, 1973
Reptilia			
Callosaurus draconoides	55.3	9.5	Irschick and Jayne, 1999
Cnemidophorus tigris	37.6	17.3	
Varanus gouldi	18.6	429	Clemente et al., 2009
Varanus giganteus	12.9	2970	
Mammalia			
Gazella thompsoni	24.2	20,500	
Procapra gutturosa	17.8	30,000	See Iriate-Díaz, 2002
Canis latrans	20.1	13,300	
Vulpes fulva	28.7	4800	
Acinonyx jubatus	15	20,000	
Sciurus carolinensis	31.0	500	
	30.2	76	
Ammospermophilus leucurus			

Species	v_r	M_b	References
Neotoma lepida	24.3	1100	
Mus musculus	43.9	16	
Perognathus longimenbris	39.3	8.9	
Lepus europeus (larger mammals, >35 kg)	37.1	4000	
Homo sapiens	5	85,000	
Equus zebra	7.4	300,000	
Equus burchelli	8.2	235,000	
Bison bison	5.4	865,000	
Cervus elephas	9.0	300,000	
Rangifera tarandus	12.7	100,000	
Gazella granti	16.7	62,500	
Antilocapra americana	21.6	50,000	
Antilope cervicapra	23.6	37,500	
Canis lupus	14.1	35,200	
Panthera tigris	7.2	161,000	
Panthera leo	8.2	156,000	
Crocuta crocuta	13.5	52,000	

[M], Mass estimated from other literature.

[L], Length estimated from other literature.